



HAL
open science

Self-Propulsion of Chemically Active Droplets

Sébastien Michelin

► **To cite this version:**

Sébastien Michelin. Self-Propulsion of Chemically Active Droplets. Annual Review of Fluid Mechanics, 2023, 55 (1), pp.77-101. 10.1146/annurev-fluid-120720- . hal-04074071

HAL Id: hal-04074071

<https://polytechnique.hal.science/hal-04074071>

Submitted on 19 Apr 2023

HAL is a multi-disciplinary open access archive for the deposit and dissemination of scientific research documents, whether they are published or not. The documents may come from teaching and research institutions in France or abroad, or from public or private research centers.

L'archive ouverte pluridisciplinaire **HAL**, est destinée au dépôt et à la diffusion de documents scientifiques de niveau recherche, publiés ou non, émanant des établissements d'enseignement et de recherche français ou étrangers, des laboratoires publics ou privés.



Distributed under a Creative Commons Attribution 4.0 International License

Self-Propulsion of Chemically Active Droplets

Sébastien Michelin

LadHyX, CNRS UMR 7646, Ecole Polytechnique, Institut Polytechnique de Paris, Palaiseau, France; email: sebastien.michelin@ladhyx.polytechnique.fr

Annu. Rev. Fluid Mech. 2023. 55:77–101

First published as a Review in Advance on
October 31, 2022

The *Annual Review of Fluid Mechanics* is online at
fluid.annualreviews.org

<https://doi.org/10.1146/annurev-fluid-120720-012204>

Copyright © 2023 by the author(s). This work is licensed under a Creative Commons Attribution 4.0 International License, which permits unrestricted use, distribution, and reproduction in any medium, provided the original author and source are credited. See credit lines of images or other third-party material in this article for license information.

Keywords

microswimmers, active droplets, Marangoni flows, advection–diffusion, viscous flows, symmetry-breaking

Abstract

Microscopic active droplets are able to swim autonomously in viscous flows. This puzzling feature stems from solute exchanges with the surrounding fluid via surface reactions or their spontaneous solubilization and from the interfacial flows resulting from these solutes' gradients. Contrary to asymmetric active colloids, these isotropic droplets swim spontaneously by exploiting the nonlinear coupling of solute transport with self-generated Marangoni flows; such coupling is also responsible for secondary transitions to more complex individual and collective dynamics. Thanks to their simple design and their sensitivity to physico-chemical signals, these droplets are fascinating to physicists, chemists, biologists, and fluid dynamicists alike in analyzing viscous self-propulsion and collective dynamics in active-matter systems, developing synthetic cellular models, or performing targeted biomedical or engineering applications. I review here the most recent and significant developments of this rapidly growing field, focusing on the mathematical and physical modeling of these intriguing droplets, together with their experimental design and characterization.

ANNUAL
REVIEWS **CONNECT**

www.annualreviews.org

- Download figures
- Navigate cited references
- Keyword search
- Explore related articles
- Share via email or social media

Phoretic flows:
slip-driven interfacial
flows resulting from
surface physico-
chemical gradients

1. INTRODUCTION

Swimming at microscopic scales is dominated by the effect of viscosity and thus presents many characteristics that are puzzling from the perspective of our own inertial experience of swimming (Childress 1981, Lauga & Powers 2009). Overcoming the conceptual and technical challenges associated with the observation, modeling, and manufacturing of microswimmers has mobilized biologists, physicists, and applied mathematicians since early observations and modeling of swimming bacteria (Berg & Anderson 1973, Lighthill 1976). Over the last 15 years, designing synthetic self-propelled systems has become a central engineering challenge, for example, for biomedical or environmental applications (Nelson et al. 2010, Jurado-Sánchez & Wang 2018). This design challenge is also driven by a marked interest in the collective dynamics, self-organization, and control of microscopic systems, an ever-growing field at the crossroads between physics, fluid dynamics and biology, commonly referred to as “active matter” (Marchetti et al. 2013). In contrast with macroscopic flocks of birds or schools of fish, microswimmer suspensions offer interesting examples of passive interactions, featuring no agent-based decision-making or complex cognitive systems. Hydrodynamics plays here a critical role, as the suspending fluid mediates one of the main interaction routes among individuals, across dimensions much larger than their body size.

Drawing inspiration from biological systems, the first synthetic microswimmers strictly followed biologically inspired designs, such as beating artificial flagella and cilia (Dreyfus et al. 2005, Vilfan et al. 2009). However, miniaturization, assembly, and powering at such small scales encounter many difficulties, calling for simpler, novel designs. Spontaneous self-organization also requires independent individual swimmers and, as such, precludes the directional macroscopic forcing used in earlier proof-of-concept systems (Zhang et al. 2009).

Instead of using miniaturized energy storage and actuation of deformable structures, chemically active swimmers convert chemical energy stored internally or in their environment into interfacial flows along their surface, thus prescribing mechanical stresses on the surrounding fluid to achieve self-propulsion (Moran & Posner 2017). Their development is currently driven by various potential applications, including targeted cargo or drug delivery (Kagan et al. 2010), chemical analysis and sensing (Yi et al. 2016), and decontamination (Jurado-Sánchez et al. 2014). The most popular designs consist of coated microparticles that catalyze surface chemical reactions (e.g., H_2O_2 decomposition, enzymatic reactions) and draw their mobility from phoretic flows generated from the resulting local chemical gradients (Paxton et al. 2004, Duan et al. 2015). However, these present significant drawbacks. As they are typically a micrometer in size or smaller, the motion of such microparticles is fundamentally Brownian. Although they do not contain any moving or miniaturized components, controlled and reproducible manufacturing of them is based upon complex physico-chemical techniques (e.g., deposition), and their propulsion requires a built-in asymmetry.

Chemically active droplets are based upon the same paradigm—they combine physico-chemical activity with the local forcing of interfacial flows by chemical gradients—but overcome several of these issues. Being as simple as pure water droplets slowly dissolving in a surfactant-saturated oil phase, they swim for hours (**Figure 1**) and have attracted rapidly growing interest since the first experimental reports of their motion (Izri et al. 2014, Maass et al. 2016). Their fluid nature combined with their ability to encapsulate complex internal chemistry allows them to reproduce several cell-like behaviors, such as migration, fusion, or division (Toyota et al. 2006, Browne et al. 2010, Banno et al. 2013). They can also be used for cargo delivery (Li et al. 2018) or metal extraction (Ban et al. 2014). Despite their fascinating simplicity, understanding the fundamental principles of their self-propulsion and interactions has nevertheless proved significantly more challenging. Isotropic by design, they must spontaneously break a spatial symmetry in order to self-propel, exploiting a nonlinear coupling of their physico-chemical dynamics to the resulting

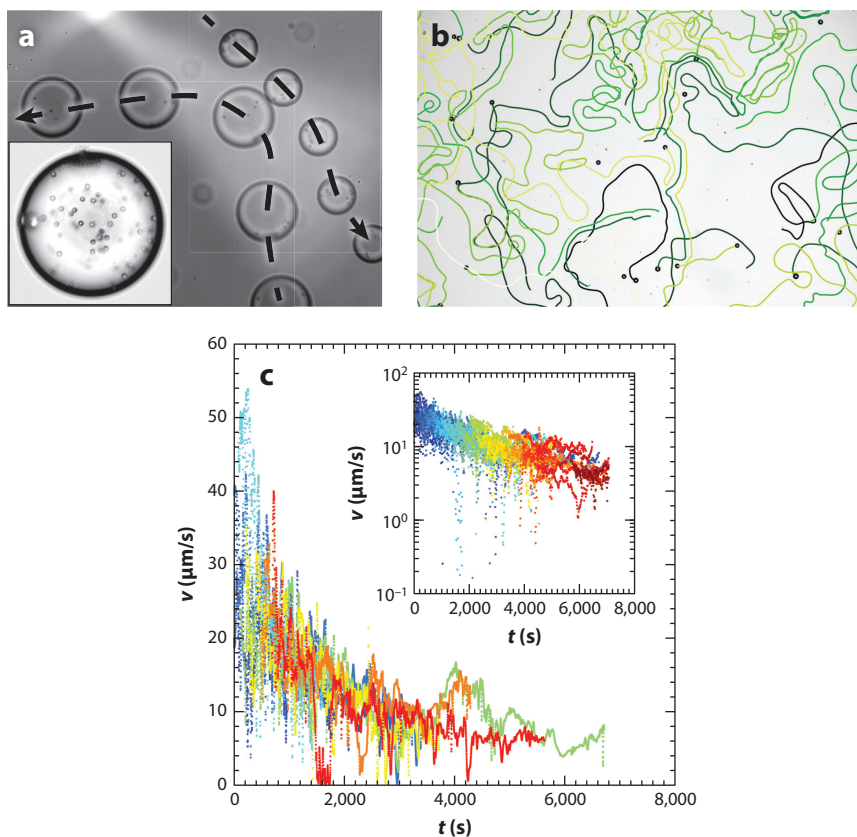


Figure 1

Self-propulsion of chemically active droplets. (*a*) Individual and (*b*) collective trajectories of swimming water droplets in monoolein-saturated squalane oil. (*c*) Evolution in time of the droplet velocities. Panels *a* and *c* adapted with permission from Izri et al. (2014), copyright 2014 American Physical Society; photo in panel *b* courtesy of O. Dauchot, M. Van der Linden, and G. Durey (Gulliver Lab, CNRS-ESPCI, Paris).

internal and external fluid motions (Morozov & Michelin 2018). This intrinsic nonlinearity and dual sensitivity to their hydrochemical environment enable complex, non-Brownian, individual, and collective motion of active droplets (**Figure 1**) but are also responsible for a significant gap between the modeling of chemically active droplets and of their rigid phoretic counterparts, for which chemical transport is mostly diffusive and decoupled from hydrodynamics.

In contrast with other Marangoni-driven self-propelled systems [e.g., camphor boats (Tomlinson 1862)], chemically active swimming droplets appeared in microfluidics labs only very recently, with most realizations reported over the last 10 years. Motivated by such rapid experimental developments and by the complexity and variety of the physico-chemical processes involved, a wealth of analysis, simulations, and modeling have been proposed over the past few years to improve our theoretical understanding. This review presents a critical panorama of this dynamic research field, combining a synthetic presentation of our current fundamental understanding of these fascinating yet complex systems, together with an overview of the evolving state of the art of their experimental design and observation. Specific focus is placed on understanding their distinctive features with respect to other chemically active swimmers—namely, the nonlinear

Reynolds number:

$Re = \rho VR/\eta$ (with η and ρ the fluid viscosity and density, respectively) measures the relative effect of inertia and viscosity on the fluid motion

Surfactants: large molecules featuring a hydrophilic head and hydrophobic tail; they adsorb preferentially at oil–water interfaces, lowering their interfacial stress (surface tension)

hydrochemical couplings at play and their consequences. Finally, we also provide an overview of the main ongoing challenges from a fluid dynamics point of view.

This review is organized as follows. After a brief reminder in Section 2 of the specific constraints and minimal ingredients for microscopic self-propulsion in a fluid medium, Section 3 presents a synthetic overview of the main experimental designs and characteristics. The fundamental hydrochemical mechanism at the heart of chemically active droplets' spontaneous self-propulsion and its modeling are presented in Section 4, together with the origin of complex individual motions. Section 5 is a review of the different interactions of active droplets, with their environment and among each other, a key step toward modeling the large-scale collective dynamics of this new type of active matter. Finally, the review concludes with some of the prominent ongoing and future challenges that must be overcome in our quest to understand the dynamics of these intriguing droplets (Section 6).

2. SELF-PROPULSION PRINCIPLES OF CHEMICALLY ACTIVE DROPLETS

2.1. Swimming at the Micrometer Scale

Chemically active droplets in the lab have a typical radius $R \sim 10\text{--}100\ \mu\text{m}$ and velocity $V \sim 1\text{--}100\ \mu\text{m/s}$. For such microswimmers, the Reynolds number is small and inertial effects are negligible: Fluid flows within and around the droplets are therefore described by the Stokes equations (Kim & Karrila 1991). The last 50 years have led to much progress in understanding and modeling the viscous propulsion of various swimming microorganisms [see the extensive and excellent reviews by Lauga & Powers (2009) and Pak & Lauga (2015)], and many of its features are applicable to any microswimmers, including swimming droplets and other active colloids.

Here we outline some of the most distinctive features of microswimmers' viscous propulsion:

1. The swimming speed is a linear function of the instantaneous forcing exerted by the microswimmer on the surrounding fluid—there is no history effect and swimming ceases as soon as the forcing disappears.
2. Net motion requires a spatially asymmetric and temporally irreversible forcing.
3. Inertia is negligible and a strict force/torque balance applies on the microswimmer at all times. In the absence of any external force (e.g., buoyancy), the total hydrodynamic force and torque thus vanish.
4. The flow perturbations introduced by a microswimmer decay slowly (algebraically), resulting in long-range interactions with other swimmers and boundaries. Force-free microswimmers are characterized by an $\mathcal{O}(1/r^2)$ hydrodynamic signature (stresslet).

2.2. Generating Interfacial Stresses and Flows

Viscous propulsion critically relies on the ability to force the surrounding fluid into motion irreversibly. Swimming cells and other biological swimmers achieve this by performing successions of shape changes (known as strokes), most commonly through the beating of active filaments (flagella, cilia) anchored on the cellular membrane (Brennen & Winet 1977, Lauga 2016). This is also a central strategy of many artificial microswimmers designed in the lab (e.g., Nelson et al. 2010, Palagi & Fischer 2018). Chemically active particles or droplets exploit instead physico-chemical gradients and short-range interactions with the surrounding fluid to generate interfacial flows along their boundaries (Anderson 1989).

The surface of a swimming droplet separates two immiscible fluids containing dissolved ionic or neutral solutes and is most often laden with large surfactants. The interaction of the different molecular species (solute, solvents, and surfactants) is incredibly complex. Yet, because such

interactions are limited to the immediate vicinity of the interface, whose thickness is typically orders of magnitude smaller than the droplet's size, these molecular interactions can be accounted for in the mesoscopic point of view of fluid mechanics through (a) an interfacial stress $\boldsymbol{\tau}_s = \nabla_s \gamma$, with $\gamma(\mathbf{r})$ the surface tension, and (b) a phoretic slip velocity \mathbf{u}_s (Anderson 1989), so that boundary conditions at the surface of the droplet for the velocity and stress of the outer and inner fluids, $\mathbf{u}^{o,i}$ and $\boldsymbol{\sigma}^{o,i}$, respectively, are

$$[\boldsymbol{\sigma}^o - \boldsymbol{\sigma}^i] \cdot \mathbf{n} = -\boldsymbol{\tau}_s, \quad \mathbf{u}^o - \mathbf{u}^i = \mathbf{u}_s. \quad 1.$$

Both \mathbf{u}_s and $\boldsymbol{\tau}_s$ are directly linked to local physico-chemical gradients at the droplet interface and drive net phoretic and/or Marangoni flows around the droplet, providing the mechanical forcing (mobility) that propels the droplet through the viscous fluid.

2.3. Minimum Ingredients for Phoretic/Marangoni Propulsion

Phoretic and Marangoni migration of passive colloids resulting from externally imposed physico-chemical gradients is a classical problem (Anderson 1989). The distinguishing feature of self-propelled active colloids lies in their ability to create and act on such local gradients themselves through a surface activity of various origins (see Section 3).

In addition to a dual activity and mobility, self-propulsion requires breaking spatial symmetry. Being intrinsically isotropic, chemically active droplets cannot rely on built-in asymmetries, a stark contrast with rigid phoretic particles (Moran & Posner 2017). Active droplets exploit instead the convective transport of the product of their activity to maintain/reinforce interfacial propelling flows in a spontaneous symmetry-breaking (Figure 2).

3. CHEMICALLY ACTIVE DROPLETS IN THE LAB

This review is dedicated to colloidal droplets that self-propel due to self-generated interfacial flows resulting from surface physico-chemical gradients (solute, temperature, etc.). Many recent examples of such chemically active droplets have been proposed in the lab and can be broadly classified into two main categories: (a) reacting droplets and (b) solubilizing droplets (Herminghaus et al. 2014, Maass et al. 2016). The former typically exploit chemical reactions to alter the structure of surfactant molecules at their interface, modifying their tensio-active properties. In contrast, the latter rely on micellar dissolution into their surfactant-saturated environment. Both mechanisms affect the droplet's surface tension and may therefore lead to self-induced Marangoni flows and propulsion of the droplet.

3.1. Reacting Droplets

Reacting droplets modify their surface tension distribution using internal or surface reactions to produce or alter surfactant molecules covering their surface. The dynamics of internal reactions is essentially independent from the outer environment, in contrast with surface reactions, where chemical reagents are transported within each phase and brought into contact at the interface only. In that case, propulsion itself is controlled by the surfactant concentration at and near the droplet surface. The possibility of encapsulating complex chemical reactions makes reacting droplets particularly well suited for targeted applications. Popular examples are listed below:

1. The internal reaction (a) can lead to the production of surfactant molecules, e.g., of a cationic surfactant inside an oil droplet via a catalytic cyclo-addition (Kasuo et al. 2019).
2. In surfactant bromination, the tensio-active properties of the surfactant (e.g., monoolein) are altered by the bromination of an unsaturated bond in its hydrocarbon chain. Bromine

Marangoni flows:
stress-driven
interfacial flows
resulting from surface
tension gradients at
fluid–fluid interfaces

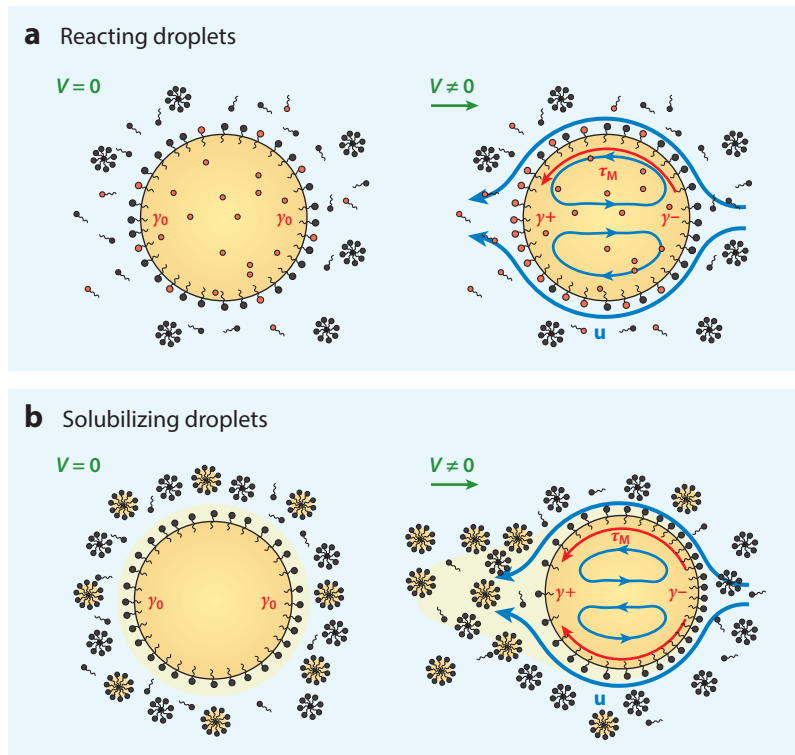


Figure 2

(Left) Isotropic nonmotile equilibrium and (right) symmetry-breaking and self-propulsion of two canonical examples of chemically active droplets. (a) Reacting droplets: A chemical (red) produced inside the droplet reduces the tensio-active properties of the adsorbed surfactant molecules. Regions of converging surface flows are rich in altered (red) surfactant molecules (increased surface tension), while diverging surface flows replenish the surface with pristine (black) surfactant (reduced surface tension), thus enhancing the fluid and droplet motions. (b) Self-solubilizing droplets: The droplet's fluid is transferred near the surface into swollen micelles, reducing the local surfactant concentration. The accumulation of swollen micelles in the wake of the moving droplet thus maintains the interfacial stress (red arrows) and Marangoni flow (blue arrows) driving the droplet's motion.

can be loaded initially inside the droplet (Suematsu et al. 2019) or produced internally via steady or oscillatory Belouzhov–Zhabotinsky (BZ) reactions, depending on the droplet composition (Thutupalli et al. 2011, Thutupalli & Herminghaus 2013, Suematsu et al. 2016).

3. pH-controlled hydrolyzation of an ester-containing surfactant in contact with the aqueous phase produces a more active surfactant complex (Banno et al. 2011, Ban et al. 2013). The reaction kinetics, and thus the droplet's propulsion properties (e.g., duration, speed), may be tuned via the pH of the aqueous outer phase.

3.2. Solubilizing Droplets (Spontaneous Emulsions)

In a second popular route to self-propulsion, active droplets dissolve spontaneously into the surfactant-saturated outer phase in a mechanism known as micellar dissolution (Herminghaus et al. 2014, Maass et al. 2016). This somewhat simpler physical chemistry has been particularly

attractive for fundamental studies of droplet motion and interactions. The mechanism is described below for oil-in-water droplets, but a similar mechanism is also available to water-in-oil droplets.

Above the critical micellar concentration (CMC), some of the droplet's oil is spontaneously transferred into empty micelles present in the vicinity of the droplet's surface, together with additional surfactant monomers, forming larger swollen micelles. This process therefore alters the local surface tension and constitutes the gradient-inducing activity required for propulsion. Micelle swelling and droplet dissolution are complex physico-chemical processes beyond the scope of this review, but they follow either (a) a micellar pathway, where micelles are filled directly at the droplet's surface, or (b) a molecular pathway, where swollen micelles are formed from dissolved oil molecules present in the surface vicinity (see Herminghaus et al. 2014).

A popular system consists in the dissolution of 4-pentyl-4'-cyanobiphenyl oil droplets in a saturated aqueous solution of tetradecyltrimethylammonium bromide surfactant (Peddireddy et al. 2012, Seemann et al. 2016). This liquid crystalline (LC) oil is nematic at room temperature. However, nematic ordering is not necessary for the droplet propulsion: Swimming is maintained above the nematic-to-isotropic transition (Krüger et al. 2016a) and is also observed for non-nematic LC oils [such as CB15 (Hokmabad et al. 2021)] or non-LC oils such as diethyl phthalate (Moerman et al. 2017, Izzet et al. 2020) or bromodecane (Cheon et al. 2021). Nematic ordering further provides an interesting visualization tool of the droplet's internal structure during the motion (Herminghaus et al. 2014, Thutupalli et al. 2018).

A similar micellar dissolution also powers the propulsion of water droplets in surfactant-saturated oil (see Izri et al. 2014, de Blois et al. 2019, Suda et al. 2021), such as monolein-saturated squalane; since this is also the combination used for BZ droplets (Thutupalli et al. 2011), micellar solubilization may therefore coexist with chemically driven propulsion for this system (Suematsu et al. 2021). More complex physico-chemical routes have also been explored for the droplet's spontaneous dissolution, such as the shedding of larger fluid vesicles at the back of the propelling droplet (Toyota et al. 2006, 2009).

3.3. Symmetry-Breaking and Other General Marangoni Swimmers

A key feature of all these examples is the intrinsic isotropy of active droplets, which must rely on the nonlinear solute transport dynamics to break symmetry. Other swimmers rely on the same physical principles, such as isotropic Marangoni surfers propelling at a fluid interface (Ender et al. 2021, Boniface et al. 2019). However, such systems also show fundamental differences in that Marangoni flows are generated along the entire fluid interface instead of the sole swimmer's surface, playing a major role in its propulsion (Boniface et al. 2021).

4. SELF-PROPULSION OF AN ISOLATED DROPLET: FUNDAMENTAL MECHANISMS AND MODELING

4.1. Modeling Chemically Active Droplets

Given such experimental diversity, it should be no surprise that modeling the self-propulsion of chemically active droplets remains an important challenge and follows various approaches. We summarize below their common characteristic features, together with a simple reference model and possible variants.

4.1.1. Hydrochemical transport. Self-propulsion of chemically active droplets emerges from the nonlinear coupling of (a) the transport of the different chemical solutes around the droplet and (b) the viscous fluid motion resulting from the interfacial forcing introduced by these solutes'

Critical micellar concentration (CMC):

maximum concentration of surfactant monomers in a given solvent; excessive surfactant monomers form supramolecular aggregates (micelles) to shield their head or tail from the solvent

gradients. Originating in the slow diffusion of the large solutes, this nonlinear hydrochemical coupling is essential to the emergence of directed self-propulsion of intrinsically isotropic droplets.

The detailed propulsion mechanism is still not completely understood, in large part due to the complexity of the physico-chemical processes and the variety across experimental systems. Yet, key common features are found in most cases, including a dual activity and mobility. The modeling of the active droplet and of its self-propulsion can be broadly rationalized along two main classes of mechanisms and models.

4.1.1.1. Interfacial hydrochemical dynamics. Interfacial hydrochemical dynamics is best suited for the description of reacting droplets, for which a reaction takes place at the interface (Thutupalli et al. 2011, Schmitt & Stark 2013): The activity of the droplet may then consist in the alteration/degradation of the pristine surfactant with a consumption rate directly related to its local concentration at the interface. The different surfactant molecules are transported along the interface by the solute-induced Marangoni flows. Locally converging surface flows drive an outward radial flow into the bulk, reducing the influx of pristine surfactant from the saturated solvent and its local surface concentration. By raising the local surface tension, this enhances the initial flow perturbation in a self-reinforcing mechanism at the origin of the spontaneous onset of propulsion (**Figure 2a**). By effectively introducing a spatially dependent activity directly driven by the surface flow divergence, this tightly coupled hydrochemical dynamics resembles the problem of surface-mobile enzymes (de Corato et al. 2020).

A simple hydrochemical model of such a mechanism writes for the reaction–advection–diffusion dynamics of the relative surface concentration of the pristine surfactant (Thutupalli et al. 2011, Schmitt & Stark 2013) with the convecting surface flow obtained by solving Stokes’ equations inside and outside the droplet in linear response to the Marangoni forcing (Morozov & Michelin 2019a, Schmitt & Stark 2013, 2016).

4.1.1.2. Bulk hydrochemical dynamics. In contrast, the activity of self-solubilizing droplets consists in the exchange of chemical species between the droplet’s surface and the outer fluid. Resulting surface tension inhomogeneities drive Marangoni flows (mobility) and a bulk transport of these chemical species. Equivalently, such micellar solubilization can be broadly interpreted as the consumption of a surface-tension-reducing solute (empty micelles and adsorbed monomers) or the production of a surface-tension-increasing one (swollen micelles). It can also be seen as an effective reduction of the local CMC (and surfactant monomer concentration) due to the presence of small amounts of dissolved oil molecules transported by the flow in the droplet’s vicinity (Izzet et al. 2020). Focusing on the second interpretation, a small droplet displacement thus results in the convective solute transport and accumulation in the droplet’s wake; the Marangoni flow driven by the resulting increased surface tension is then able to propel the droplet forward (**Figure 2b**).

More complete models also couple the interfacial and bulk transports through the description of the adsorption/desorption dynamics of surfactant molecules from the interface (Rednikov et al. 1994a, Yoshinaga et al. 2012, Morozov 2020): The two classes presented above can then be viewed, at least qualitatively, as limit cases of the sorption kinetics of the surfactant species. As temperature changes also alter surface tension, most of the above discussion of chemically active droplets remains applicable for heat-releasing droplets (Rednikov et al. 1994c).

All models share common and essential characteristics for spontaneous propulsion:

1. Destabilization: Local physico-chemical surface gradients (e.g., temperature or solute content) generate an interfacial flow, and the associated convective chemical transport enhances the initial inhomogeneity.

2. Threshold: Self-sustained convective transport of the field must dominate over chemically driven or diffusion-driven relaxation toward equilibrium.

4.1.2. Marangoni versus phoretic forcing. For simplicity, the presentation above focused specifically on Marangoni-driven flows. However, linear modeling of the surface tension dependence is only valid for low surfactant coverage. Furthermore, phoretic slip may also develop at a fluid–fluid interface in the presence of a solute concentration, and the balance between both processes is determined by the detailed molecular interactions, the surfactant coverage density, or the viscosity ratio. A more general approach thus appears necessary and consists in retaining both drivings for the interfacial flow (Morozov & Michelin 2019a). In that regard, results on phoretic propulsion at finite or large Pe (obtained from a somewhat simpler model that does not require describing the internal fluid’s motion) are also likely relevant to the droplet problem (Yariv 2016, Yariv & Kaynan 2017, Saha et al. 2021, Chen et al. 2021). The resulting dynamics in either case are indeed essentially the same for moderate Pe (Michelin et al. 2013, Izri et al. 2014), but significant differences have been identified for larger Pe [e.g., subsequent bifurcations and transition to chaos; see Morozov & Michelin (2019a) and Lin et al. (2020)].

4.1.3. Relaxation dynamics. Individual models differ in their description of the solute’s relaxation. In interfacial mechanisms, this relaxation originates in surface diffusion, degradation, or desorption from the surface (Thutupalli et al. 2011, Schmitt & Stark 2013, de Corato et al. 2020). For bulk mechanisms, relaxation stems from a bulk degradation (Yoshinaga et al. 2012) or diffusive/convective transport away from the particle (Izri et al. 2014, Morozov & Michelin 2018, Picella & Michelin 2022). The presence (or not) of a bulk relaxation significantly impacts the localization of the chemical footprint of the droplet by introducing an effective exponential screening length for the solute concentration, instead of its diffusion-induced algebraic decay away from the droplet. The resulting chemically mediated interactions of active droplets with surrounding boundaries or with other droplets may be significantly altered (Lipperra et al. 2020b, 2021; Yabunaka & Yoshinaga 2016).

4.1.4. Droplet deformability. Being liquid, active droplets are expected to deform in response to the viscous stresses applied by the inner and outer flows, with relative deformations of the order of $Ca \sim \eta\mathcal{V}/\gamma$, with \mathcal{V} , η , and γ the typical relative flow velocity, fluid viscosity, and surface tension, respectively. The models outlined previously can be directly generalized to account for these, at least in the limit of small deformability (Rednikov et al. 1994b, Yoshinaga 2014, Morozov & Michelin 2018). However, in most experimental situations $Ca \ll 1$ justifies focusing on purely spherical droplets.

4.2. A Reference Model

Keeping in mind these possible variations, we outline below a simple advection–diffusion model for the bulk transport of a chemical solute emitted from the surface of the moving active droplet into the outer fluid (Michelin et al. 2013, Morozov & Michelin 2019a). This model has served as a growingly popular reference for understanding these systems. Despite likely shortcomings in the description of the droplet’s interfacial physico-chemical properties, its simplicity has recently motivated and facilitated much fundamental understanding of this rich system (Saha et al. 2021), as well as investigations of droplet–droplet interactions (Lipperra et al. 2020a,b), confinement effects (Desai & Michelin 2021, Picella & Michelin 2022), complex unsteady dynamics (Morozov & Michelin 2019b, Hokmabad et al. 2021), and transition to chaotic motions (Morozov & Michelin 2019a, Hu et al. 2019, Chen et al. 2021).

4.2.1. Hydrochemical transport equations. The transport equations for the inner and outer fluid flows $\mathbf{u}^{o,i}$ and the concentration perturbation C in the outer fluid are

$$\frac{\partial C}{\partial t} + \mathbf{u}^o \cdot \nabla C = D \nabla^2 C, \quad \eta_{o,i} \nabla^2 \mathbf{u}^{o,i} = \nabla p^{o,i}, \quad \nabla \cdot \mathbf{u}^{o,i} = 0. \quad 2.$$

The droplet has radius R , and its activity and Marangoni/phoretic mobility further impose

$$D \mathbf{n} \cdot \nabla C = -\mathcal{A}, \quad \mathbf{u}^o - \mathbf{u}^i = \mathcal{M} \mathbf{n}^\perp \cdot \nabla C, \quad \mathbf{n}^\perp \cdot [(\boldsymbol{\sigma}^o - \boldsymbol{\sigma}^i) \cdot \mathbf{n} + \gamma_c \nabla C] = 0 \quad 3.$$

on the droplet's surface, with $\boldsymbol{\sigma}^{o,i}$ the associated Newtonian fluid stress tensor. Here, \mathcal{A} accounts for a fixed-flux emission of solute of diffusivity D , $\gamma_c = (\partial \gamma / \partial C)$ is the surface tension sensitivity to solute gradients, and \mathcal{M} is the phoretic mobility. In unbounded domains, the concentration and flow perturbations decay far from the droplet (i.e., $C, \mathbf{u}^{o,i} \rightarrow 0$ for $|\mathbf{r}| \gg R$) and the impermeability of the droplet imposes $\mathbf{u}^{o,i} \cdot \mathbf{n} = \mathbf{V} \cdot \mathbf{n}$ on \mathcal{S} . The droplet's velocity \mathbf{V} is then obtained from the force balance (inertia is negligible at such scales), so that in the absence of any external force we have

$$\mathbf{F}_b = \int_{\mathcal{S}} \boldsymbol{\sigma}^o \cdot \mathbf{n} \, dS = \mathbf{0}. \quad 4.$$

Note that these conditions can be modified straightforwardly to account for an external force (e.g., buoyancy) or inhomogeneous chemical or hydrodynamic backgrounds.

4.2.2. Péclet number. This model features three important nondimensional parameters:

$$\text{Pe} = \frac{\mathcal{V}R}{D}, \quad \tilde{m} = \frac{\eta_i \mathcal{M}}{\gamma_c R}, \quad \tilde{\eta} = \frac{\eta_p}{\eta_i}, \quad 5.$$

with \mathcal{V} the characteristic magnitude of the activity-driven interfacial flows (e.g., $\mathcal{V} = \mathcal{A} \mathcal{M} / D$). The Péclet number Pe is a relative measure of convective-to-diffusive solute transport; the mobility ratio \tilde{m} compares the role of phoretic and Marangoni forcings, and $\tilde{\eta}$ is the viscosity ratio. The limit of a pure droplet is recovered for $\tilde{m} \ll 1$, and that of a phoretic particle for $\tilde{m} \gg 1$ and $\tilde{\eta} \ll 1$ (Morozov & Michelin 2019a).

The Péclet number is also a relative measure of the droplet's activity or mobility magnitude, or of the droplet's size. It is sometimes referred to as the Marangoni number in order to distinguish it from the same quantity built on the a priori unknown droplet velocity V instead of the intrinsic velocity scale \mathcal{V} .

4.3. Symmetry-Breaking and the Emergence of Self-Propulsion

Chemically active droplets present no intrinsic asymmetry. A nonmoving isolated active droplet thus modifies its chemical environment isotropically ($\bar{C} = \mathcal{A} R^2 / r$) and its surface concentration remains uniform, resulting in no fluid or droplet motion regardless of Pe . Droplet propulsion thus necessarily involves a spontaneous symmetry-breaking, which stems from the nonlinear hydrochemical coupling introduced by the convective transport.

4.3.1. Stability of the isotropic state. The stability analysis of the reference model (Equations 2–4) around this nonpropelling regime confirms the qualitative arguments outlined above. A discrete set of increasing critical thresholds, $\text{Pe}_c^{(n)}$, is identified for force-free droplets, beyond which specific axisymmetric modes of increasing azimuthal order n become successively unstable as diffusion becomes too slow to counteract the amplifying effect of the convective coupling (Figure 3a). The unstable mode associated with the lowest threshold, $\text{Pe}_c^{(1)}$, is dipolar and the only one associated with a net droplet motion; $[\text{Pe}_c^{(n)}]_{n \geq 2}$ correspond to flow-stirring modes by

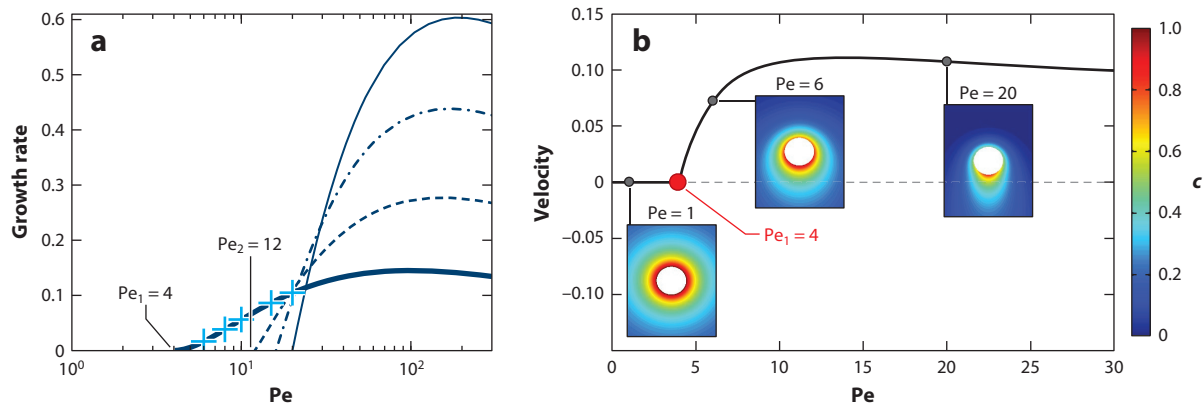


Figure 3

Symmetry-breaking and onset of droplet motion. (a) Linear growth rate of the successive unstable modes of the isotropic equilibrium. (b) Evolution with Pe of the active droplet's velocity and of its chemical footprint, obtained from numerical simulations of the reference nonlinear hydrochemical model. Self-propulsion occurs for $Pe \geq Pe_1 = 4$. Abbreviation: Pe , Péclet number. Panel *a* adapted with permission from Michelin et al. (2013); copyright 2013 AIP Publishing. Panel *b* adapted with permission from Izri et al. (2014); copyright 2014 American Physical Society.

a nonmoving force-free droplet (Izri et al. 2014; Morozov & Michelin 2018, 2019a; Hokmabad et al. 2021). For tethered droplets, $Pe_c^{(1)}$ is replaced by an alternative threshold Pe_c^* , corresponding to fluid pumping by a fixed droplet exposed to a net external force (Rednikov et al. 1994a).

The self-propelling mode always becomes unstable first for spherical droplets: Droplet motion toward lower solute concentration and the resulting surface flow divergence enhance the destabilizing front-back contrast in solute distribution. Significant droplet deformability promotes the instability of higher-order modes with similar symmetry, potentially modifying the thresholds' ordering for larger Ca (Yoshinaga 2014, Morozov & Michelin 2018).

4.3.2. Near-threshold dynamics and bifurcation characteristics. For $Pe > Pe_c^{(1)}$, small perturbations of the isotropic state grow exponentially then saturate under the nonlinear effect of hydrochemical coupling (Figure 3b). All directions being a priori equivalent, the direction of motion is thus chosen by the initial perturbation (Saha et al. 2021). Numerical solution of the full nonlinear model provides the bifurcation curve, indicating the emergence of a new stable branch with $V \neq 0$ above $Pe_c^{(1)}$ as the isotropic state (with $V = 0$) becomes unstable (Figure 3b). Steady self-propulsion is associated with a self-sustained accumulation of solute in the wake of the droplet and the development of a sharp boundary layer at the front of the droplet as Pe is increased.

Weakly nonlinear analysis shows $V \sim Pe - Pe_c^{(1)}$ at the propulsion onset, instead of the classical square-root behavior of supercritical pitchfork bifurcations (Morozov & Michelin 2018). This in fact points to the singular behavior of the advection-diffusion problem for small droplet velocity in unbounded domains (Farutin & Misbah 2021): Advection is subdominant with respect to diffusion in the near-field [i.e., for $r = \mathcal{O}(R)$] but must be retained at leading order in a far-field boundary layer [$r = \mathcal{O}(PeV)$], resulting in a symmetry-preserving pseudo-quadratic dominant correction of the amplitude equations, $dV/dt = \sigma V - K|V|V$ (Vélarde et al. 1996).

The exact nature of the bifurcation thus depends on the details of the model considered: The convective far-field boundary layer is absent when chemical transport is restricted to the droplet surface, or when the chemical field at large distances is screened by bulk degradation (Yoshinaga et al. 2012) or finite domain sizes (Misbah et al. 2021), thus leading to a classical pitchfork

bifurcation. Subcritical transition may also be obtained when other nonlinear corrections are included [e.g., surface coverage saturation (de Corato et al. 2020)] or when the droplet’s activity is concentration dependent (Rednikov et al. 1994a).

4.4. Complex Dynamics of Isolated Droplets

Balistic motion is observed in specific experimental conditions [e.g., for $Pe \gtrsim Pe_c^{(1)}$ (Suga et al. 2018, Izzet et al. 2020, Hokmabad et al. 2021)], but complex motions of chemically active droplets are commonly observed for more general settings (**Figure 4**), for example, by changing the surfactant’s saturation of the outer phase (Ban et al. 2012), its chemical structure (Banno et al. 2013), its affinity to the outer phase (Hirono et al. 2018), or the droplet’s internal chemical state (Suematsu et al. 2021).

4.4.1. Secondary transitions and mode-switching. Recent experiments provide some insight into the complex dynamics using well-monitored changes in experimental conditions. Increasing the droplet’s size (Suga et al. 2018, Suda et al. 2021, Hokmabad et al. 2022a) or its effective activity [e.g., solute, surfactant, or reactant addition (Izzet et al. 2020, Dwivedi et al. 2021b, Suematsu et al. 2021, Hokmabad et al. 2022b)], or reducing the solvent’s viscosity (Hokmabad et al. 2021) effectively increases Pe and triggers unsteady motion, curved trajectories, and erratic changes (**Figure 4a,b**).

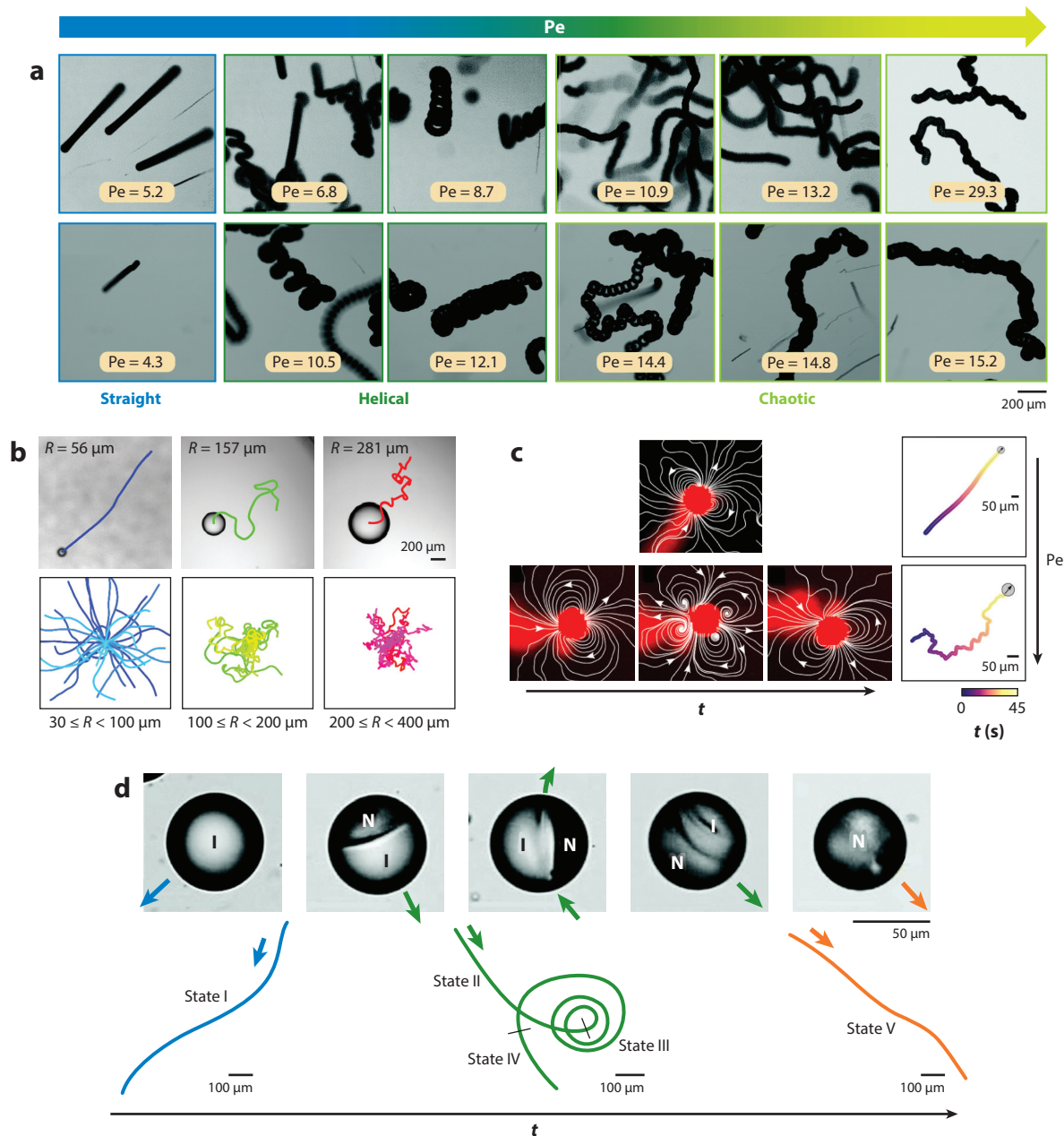
These can be understood as secondary transitions affecting the self-propelled steady state of the reference model (Section 4.2). The dipolar mode is the only unstable one for lower Pe , but higher-order modes become successively unstable for increasing Pe , leading to the possible coexistence of several unstable modes with different polar symmetries and associated with significantly different droplet behaviors (Morozov & Michelin 2019a). Transitions between motile and nonmotile states may be triggered by droplet collisions (Lipperera et al. 2020a) or occur spontaneously under the effect of fluctuations or solute accumulation in the droplet’s environment (Hokmabad et al. 2021): The resulting dynamics is bimodal (“stop-and-go”) as the droplet continuously switches from a (dipolar) propelling mode to a (quadrupolar) stopping/reorienting mode (**Figure 4c**).

Droplet shrinking is too slow to impact the propulsion dynamically (Izri et al. 2014) but enables a quasi-steady scan of a wide range of sizes during a single experiment: Large droplets initially display complex random-like behavior before switching to ballistic motion and finally stopping altogether as R (and thus Pe) is reduced (Suga et al. 2018).

4.4.2. Emergence of chaotic behavior. Decorrelation of the droplet’s orientational dynamics is observed as Pe is increased further, with erratic or chaotic-like motion reported experimentally (Dwivedi et al. 2021b, Hokmabad et al. 2021) and numerically (Morozov & Michelin 2019a, Lin et al. 2020, Chen et al. 2021). Quantitative insights into possible chaotic transitions have so far been obtained for constrained geometries: For axisymmetric motion of the droplet, Morozov & Michelin (2019a) observed the emergence of a symmetric and quadrupolar pumping mode (no propulsion), followed by a chaotic motion for increasing Pe . They showed that such a large- Pe transition is promoted by the presence of a chemically induced slip at the droplet surface and is in fact absent for purely Marangoni forcing. Using a 2D ansatz (a “cylindrical” droplet), Hu et al. (2019) observed successive and increasingly close transitions leading to a fully chaotic regime.

However, these do not fully represent generic 3D motions. Axially constrained droplets must fully stop and run into their own chemical wakes to change direction (Morozov & Michelin 2019a). To be well posed, 2D analyses require a finite-distance chemical screening whose size directly controls the motion onset or its characteristics (Hu et al. 2019). This calls for a more complete characterization of secondary instabilities and chaotic transition.

4.4.3. Chemically driven dynamics. Complex internal chemistry may also directly trigger intricate individual dynamics; different behaviors have indeed been observed for the much studied BZ droplets, depending on the exact internal composition and chemical state: (a) slow and persistent motion, when no bromine is present (Izri et al. 2014, Suematsu et al. 2021); (b) fast and reorienting propulsion, for a fixed supply or steady bromine production (Thutupalli et al. 2011,



(Caption appears on following page)

Figure 4 (Figure appears on preceding page)

(a) Time-lapse trajectories of CB15 oil droplets in a TTAB (tetradecyltrimethylammonium bromide)-saturated aqueous solution for increasing surfactant concentration (*top row*) or increasing droplet size (*bottom row*). (b) Swimming time-lapse trajectories of water droplets of increasing radius R in monoolein-saturated solutions of squalane oil. (c) Experimental visualization (*left*) of the solute field (*red*) and streamlines (*white*) generated by a self-propelled CB15 oil droplet solubilizing in an aqueous solution of TTAB cationic surfactant, as well as (*right*) its trajectory when the outer fluid viscosity η_o (and the Péclet number Pe) is modified by adding glycerol to the aqueous phase. (d) Visualization of transient dynamical changes of multicomponent oil droplets triggered by phase separation and internal reordering of distinct isotropic (I) and nematic (N) phases. Panel *a* adapted from Hokmabad et al. (2022a) (CC BY 3.0). Panel *b* adapted from Suda et al. (2021) with permission; copyright 2021 American Physical Society. Panel *c* adapted from Hokmabad et al. (2021) (CC BY 4.0). Panel *d* adapted from Wang et al. (2021) with permission; copyright 2021 Royal Society of Chemistry.

Suematsu et al. 2019); (c) retarded transition between these regimes (Suematsu et al. 2021); or (d) large-amplitude oscillations triggered by chemical waves (Kitahata et al. 2011, Suematsu et al. 2016). Multiphase solubilizing droplets provide another example of internal chemical control of the droplet propulsion (**Figure 4d**), with phase separation and temporal evolution of the droplet behavior triggered by solubilization differences of the droplet components (Li et al. 2018, 2020; Wang et al. 2021).

4.4.4. Internal droplet structure (liquid crystal droplets). Many experiments focus on swimming LC oil droplets (Peddireddy et al. 2012, Herminghaus et al. 2014) or shells (Hokmabad et al. 2019). While not necessary for self-propulsion, the internal nematic ordering of the droplet can significantly affect its propulsion (Krüger et al. 2016a, Suga et al. 2018). Nematic droplets feature a topological defect; as swimming develops, this defect is pushed away from its central equilibrium position, thus introducing internal stresses. The emergence of spiral trajectories may then be interpreted as a two-way coupling between an internal polarization of the nematic ordering and the hydrochemical dynamics (Morozov & Michelin 2019b). However, more recent experiments have also demonstrated that internal droplet ordering is not necessary for the emergence of such curved and complex motion, which is also observed for nonnematic droplets (Hokmabad et al. 2022a).

5. DROPLET INTERACTIONS

5.1. Chemotaxis and Reverse Autochemotaxis of Active Droplets

Active droplets introduce a chemical footprint on their environment due to their exchange of chemical solutes. In turn, chemical inhomogeneities around them induce interfacial stresses; the resulting drift and reorientation provide them with a chemotaxis similar to biological microorganisms (Berg 1975).

The self-propulsion of a solubilizing droplet is powered by the capture into empty micelles of some of its internal fluid and additional surfactant monomers from its surface vicinity to form more stable swollen micelles. A local accumulation of swollen micelles or dissolved droplet fluid (e.g., in their wake; see **Figure 5a**) therefore increases the local surface tension and pushes the droplet away from such accumulation regions (Izzet et al. 2020). As a result, active droplets feature an intrinsic reverse autochemotaxis (Maass et al. 2016) (i.e., they flee their own wake), and their dynamics is altered by other droplets or confining walls (Sections 5.2 and 5.4).

Conversely, a local increase of the bulk concentration in surfactant monomers will reduce surface tension and generate a locally diverging Marangoni flow at the droplet's surface, propelling it toward such chemically rich regions (**Figure 5b**). Jin et al. (2017) recently exploited this chemotaxis to demonstrate the droplet's maze-solving ability by its sensing of the shortest path toward the surfactant-rich exit (**Figure 5c**).

Chemotaxis:
the ability of a self-propelled system to drift or reorient as the result of a local chemical gradient

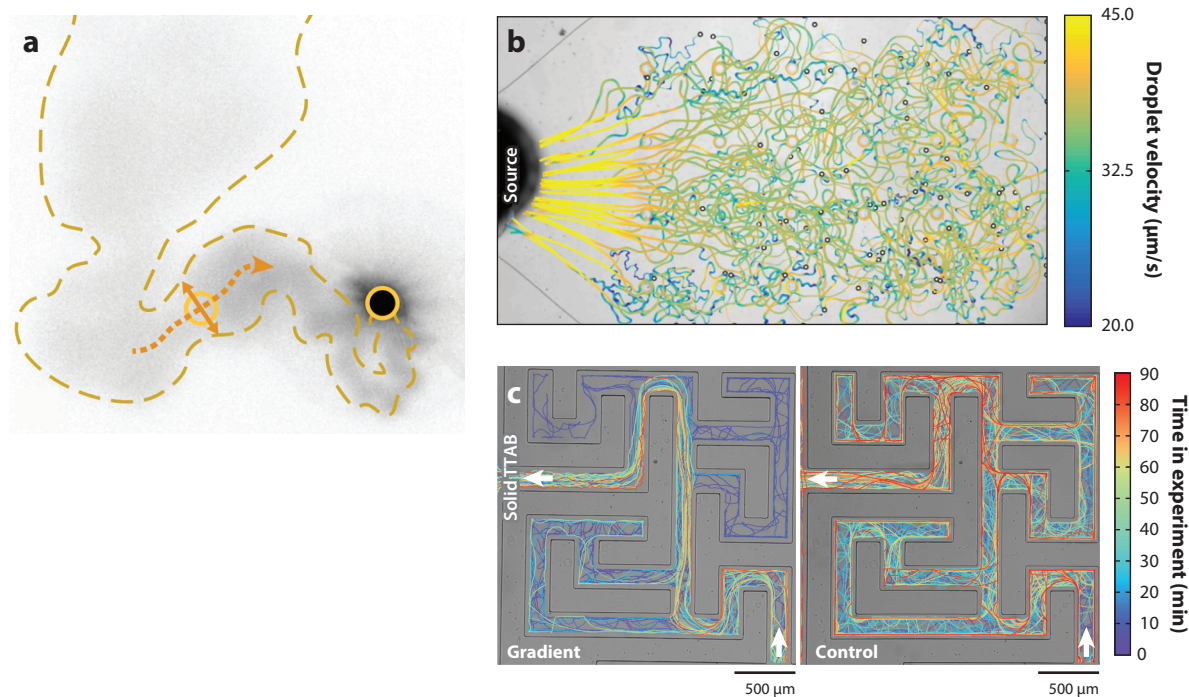


Figure 5

(a) Experimental visualization of the self-avoiding dynamics of a swimming oil droplet as a result of chemo-repulsive interactions with oil-filled micelles. (b,c) Chemotactic droplets can (b) swim toward a concentrated source of surfactant [tetradecyltrimethylammonium bromide (TTAB)] or (c) find the shortest path to a maze's entrance. Panel a adapted from Izzet et al. (2020) (CC BY 4.0). Panel b adapted from Jin et al. (2018) with permission; copyright 2018 IOP Publishing. Panel c adapted from Jin et al. (2017) with permission.

5.2. Interactions with Confining Boundaries

By preventing its diffusion away from the emitting droplet, chemically inactive boundaries result in a local solute accumulation, which profoundly modifies the flow field generated by the droplet, such as when it is maintained near a wall by buoyancy (Krüger et al. 2016a) or in Hele–Shaw cells (Figure 6a) (Dey et al. 2022): A wall-normal pumping mode develops and plays a dominant role in the hydrodynamic signature of the droplet (de Blois et al. 2019).

This accumulation effectively introduces a repulsive droplet–wall interaction, and an approaching droplet will slow down, reverse direction, and swim away. Such repulsive interactions, which are also present for phoretic colloids (Yariv 2016), dominate far-field and low-Pe interactions of active droplets with confining walls; however, the nonlinear hydrochemical coupling allows for nontrivial dynamics when convective effects become dominant in near-field or larger-Pe interactions. Using the complete model of Section 4.2 for axisymmetric collisions, Lippera et al. (2020b) demonstrated the dominance of chemical repulsion in the rebound dynamics for low-to-moderate Pe, as well as the emergence of complex unsteady rebounds for higher Pe when a fully nonlinear hydrochemical coupling becomes significant. The similar complete analysis of near-field interactions in oblique collisions remains thus far elusive, calling for a more in-depth investigation.

Indeed, swimming droplets are not systematically repelled by interfaces, as attraction to or orbiting around obstacles was also reported (Figure 6b) (Jin et al. 2019). Such capture is

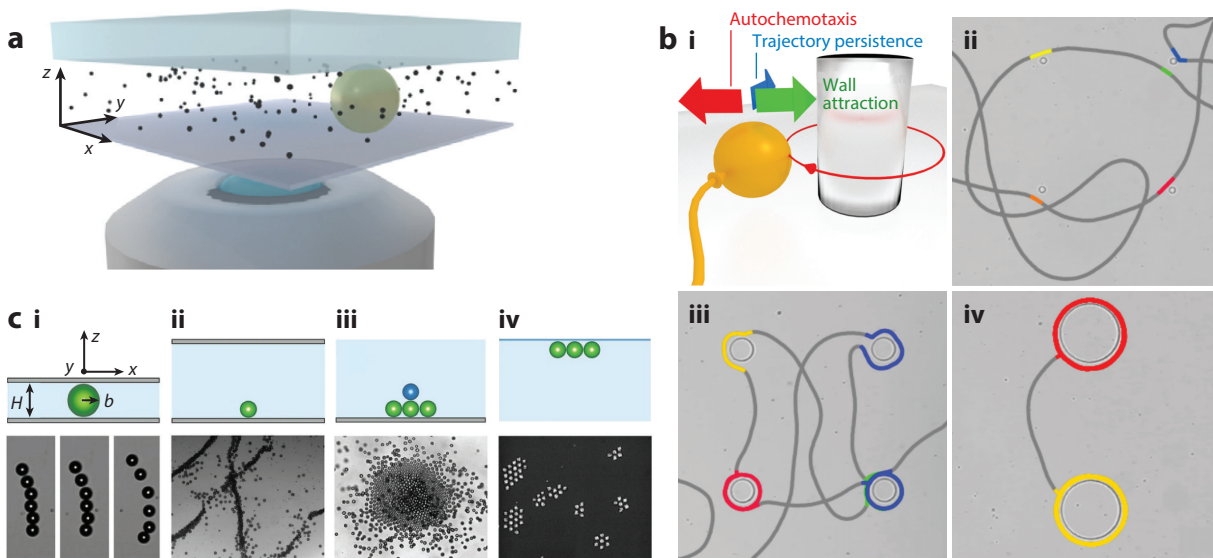


Figure 6

Droplet–wall interactions. (a) Swimming droplets are commonly studied in confined environments such as Hele–Shaw cells. (b) Trapping and guidance of oil droplets around pillars. (c) The nature and proximity of confining boundaries profoundly modify the collective dynamics and organization of active droplets. Panel *a* adapted from Jin et al. (2021) with permission; copyright 2021 American Physical Society. Panel *b* adapted from Jin et al. (2018) with permission; copyright 2018 IOP Publishing. Panel *c* adapted from Thutupalli et al. (2018) with permission.

commonly observed for swimming microorganisms, suggesting a possible hydrodynamic origin of this wall attraction (Hokmabad et al. 2022a). However, its origin and precise competition with the chemically induced repulsion remains to be fully understood. Beyond individual dynamics, the presence and nature of a boundary profoundly modify how active droplets interact with each other (**Figure 6c**) (Thutupalli et al. 2018).

Most active droplets swim in the immediate vicinity of a wall, a feature ignored in most models; a clear understanding of wall–droplet interactions and confined propulsion thus represents one of the most pressing modeling challenges on the topic (Section 6.1).

5.3. Interactions with an External Flow

Chemically active droplets placed in a flow experience a net drift and reorientation, just like passive colloids (Faxen’s law; see Kim & Karrila 1991). Combined with self-propulsion, this leads to an active directed motion in nonuniform flows (rheotaxis), examples of which abound in active matter, such as bacterial rheotaxis (Marcos et al. 2012) or up- or cross-stream migration of Janus phoretic colloids (Palacci et al. 2015, Katuri et al. 2018).

In contrast with other systems, the effect of a nonuniform flow on the trajectories of a chemically active droplet remains so far relatively unexplored. Dey et al. (2022) recently reported oscillatory trajectories and upstream migration of isotropic LC droplets inside a rectangular capillary flow; a simplified far-field model of the flow perturbation introduced by the droplet was shown to reproduce such trajectories, suggesting a purely hydrodynamic origin to this rheotactic behavior. However, this question requires further investigation due to the fundamental inability of far-field models to account for the lubrication effects present for such tightly confined geometries. Furthermore, Dwivedi et al. (2021a) reported similar dynamics in Couette flows and

Rheotaxis: the ability of a self-propelled system to drift or reorient in a local flow gradient (shear)

argued qualitatively instead for a chemical origin of the reorientation of the droplets coupled to the droplet's internal structure.

More generally, the effect of the flow-induced reorganization of the chemical distribution around the droplets remains almost entirely unexplored, despite its likely critical role on droplet propulsion. The asymptotic analysis of the far-field hydrodynamic signature of a model active colloid by a uniform shear flow is a notable exception (Yariv & Kaynan 2017), but such analysis remains limited to subcritical Pe (i.e., without any droplet propulsion).

5.4. Droplet–Droplet Interactions

Self-solubilizing droplets are both net sources/sinks of chemical solute and force-free microswimmers; they may thus generate $\mathcal{O}(1/d^2)$ hydrodynamic and chemical drifts of their neighbors. Such a dual hydrochemical signature influences the trajectories of other droplets that undergo chemotaxis and hydrodynamic interactions like many swimming cells (Lauga 2020), resulting in complex individual and collective dynamics (Figure 7).

Chemically active droplets are intrinsically antichemotactic, and therefore tend to avoid other droplets or their persistent chemical trails (Figure 7a) (Moerman et al. 2017, Jin et al. 2017). However, the nonlinear hydrochemical coupling makes the collision result particularly sensitive to its precise conditions, as illustrated by the outcome diversity and sensitivity of head-on droplet

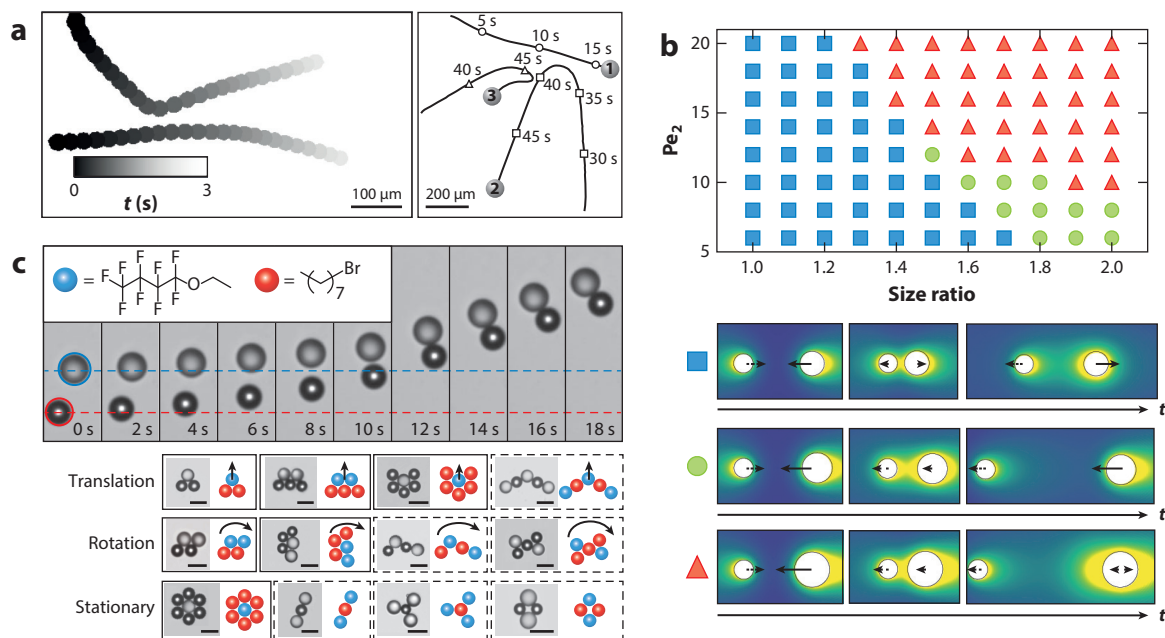


Figure 7

Droplet–droplet interactions. (a) Experimental trajectories of water-in-oil (left) or oil-in-water (right) active droplets, which are chemically repelled by other droplets and their persistent chemical trails. (b) Possible outcome of axisymmetric droplet collisions in numerical simulations of the complete model: Depending on their relative size, active droplets undergo asymmetric rebounds (blue squares), bound-state chasing regimes (green disks), or mode-switching toward a pumping mode for the largest droplet (red triangles). (c) Experimental visualization of predator–prey interactions (top) or translating, rotating, and stationary aggregate formations for droplets of different micellar solubilization rates (bottom). Scale bars are 100 μm . Panel a adapted with permission from (left panel) Moerman et al. (2017), copyright 2017 American Physical Society, and (right panel) Jin et al. (2017). Panel b adapted from Lippera et al. (2020a) with permission; copyright 2020 American Physical Society. Panel c adapted from Meredith et al. (2020) with permission; copyright 2020 Springer Nature.

collisions to small contrasts in droplet size (**Figure 7b**) (see Lippera et al. 2020a). A complete hydrochemical modeling of more generic oblique collisions remains thus far elusive, and Lippera et al. (2021) proposed instead a reduced-order model based on the dominant chemical interactions and the finite-time reorientation of the droplet’s wake, predicting and characterizing the strong sensitivity of the collision outcome (alignment or scattering) to the droplet’s initial arrangement. These results were then recently confirmed experimentally by Hokmabad et al. (2022b), further providing unique visualizations of the droplets’ chemical trails. Long-ranged repulsive chemical interactions cannot, however, explain the droplets’ long-term alignment, whose hydrodynamic origin remains to be confirmed (Hokmabad et al. 2022a). In the long term, the persistence of the droplets’ repelling chemical trails profoundly constrains the droplet trajectories and their long-time dynamics, introducing an effective caging effect (Hokmabad et al. 2022b).

Even more diverse interactions arise from variability in chemical composition: Droplets of different relative solubility or solubilization rates may effectively use each other’s wake as fuel, leading to peculiar and tunable predator–prey dynamics, as well as assembly into larger droplet clusters with distinct dynamical properties (**Figure 7c**) (Meredith et al. 2020).

5.5. Forced Motion of Active Droplets

The symmetry-breaking instability and emergence of self-propulsion can be generalized to active droplets experiencing a net nonhydrodynamic force F (e.g., gravity). This is in fact particularly relevant experimentally, as droplets are typically not neutrally buoyant. A chemically passive droplet experiences a net linear drift in response to an outer force (Stokes’ law). For a chemically active droplet (i.e., $Pe > 0$), the forcing–velocity relation becomes nonlinear (**Figure 8a**); for imposed $F \neq 0$, the Marangoni forcing resulting from the accumulation of solute in the wake of the drifting droplet enhances self-propulsion—the effective hydrodynamic drag is reduced and velocity dependent (Yariv & Kaynan 2017). As Pe is increased further, we note the emergence of (a) self-propelled force-free droplets ($F = 0, V \neq 0$) for $Pe > Pe_c^{(1)}$ corresponding to spontaneous motion, and (b) nonswimming pumping droplets ($V = 0, F \neq 0$) for $Pe > Pe_c^* > Pe_c^{(1)}$ that stir the fluid to maintain the required concentration contrast and Marangoni forcing to balance the net outer forcing (see also Rednikov et al. 1994a).

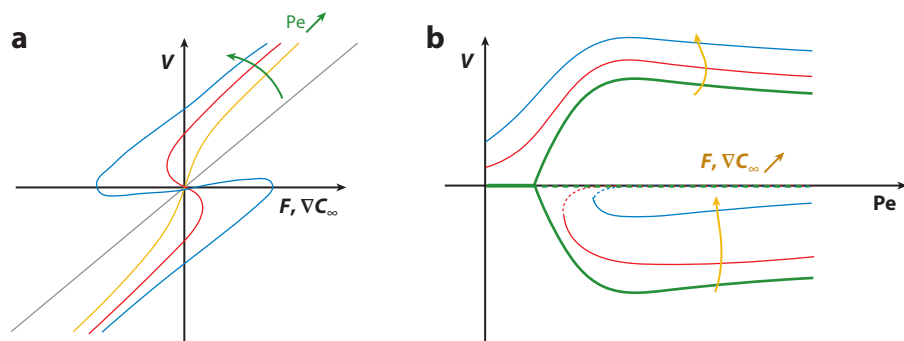


Figure 8

Spontaneous axisymmetric motion of a forced droplet obtained numerically from the reference nonlinear hydrochemical model (Section 4.2). (a) Forcing–velocity diagram. (b) Modified bifurcation diagram under the effect of a directional external forcing (external force F or background concentration gradient ΔC_∞), which breaks the intrinsic isotropy of the problem. Stable and unstable branches are denoted as solid and dashed lines, respectively. Motion always occurs in the direction induced by the forcing (upper branch), but propulsion against the forcing is also possible for sufficiently large Péclet number Pe .

This suggests an imperfect bifurcation (Saha et al. 2021), as illustrated in **Figure 8b** for axisymmetric propulsion. For $F = 0$, self-propulsion occurs spontaneously in any direction for $Pe > Pe_c^{(1)}$; an external (directional) force breaks the symmetry of the two branches. Stable propulsion along the outer force is always observed; for fixed Pe and sufficiently small F , two other solutions are found, including a stable motion against the imposed forcing, a scenario consistent with recent reports of droplet motion against gravity (Moerman 2019).

A similar framework applies to the force-free motion of active droplets in externally imposed chemical gradients, e.g., the chemical footprint of neighboring droplets (Rednikov et al. 1994c, Lippera et al. 2020b); however, the modified hydrodynamic footprint associated with the different forcing and its impact on chemical transport and induced Marangoni stresses must be accounted for carefully.

6. PERSPECTIVES: SOME OPEN PROBLEMS

In addition to the challenges already presented (e.g., large- Pe dynamics), we conclude this review with a brief overview of some open questions in the characterization and modeling of swimming droplets, and of key ongoing contributions to resolving them.

6.1. Strongly Confined Droplets

In most experiments, active droplets swim close to and along rigid walls (de Blois et al. 2019, Cheon et al. 2021) or within Hele–Shaw cells (Hokmabad et al. 2021) or even small capillaries (de Blois et al. 2021), offering a clear demonstration that large viscous stresses classically associated with lubrication layers do not hinder self-propulsion but alter their collective dynamics (Krüger et al. 2016a, Thutupalli et al. 2018). However, ignoring such intrinsic experimental features, existing models focus almost exclusively on propulsion in unbounded environments with slow (algebraic) far-field decays and long-ranged interactions. Accurate modeling of confined propulsion is thus one of the main challenges of the field.

Partially lifting the veil, Desai & Michelin (2021) recently demonstrated using the reference model that a nearby wall actually promotes the symmetry-breaking instability and onset of propulsion. Stronger confinement further results in enhanced swimming speeds (Picella & Michelin 2022), consistent with recent experimental observations inside tight capillaries (de Blois et al. 2021). Both of these theoretical studies point to two critical features of confined motion: (a) a fundamental modification of the solute's transport around and away from the droplet in order to cope with the wall-restricted solute diffusion, and (b) the localization of driving interfacial stresses to the most confined regions where hydrodynamic resistance (i.e., grip on the substrate) is largest.

6.2. Chemical Dynamics, Restricted Diffusion and Mathematical Well-Posedness

The reference model has the clear advantage of retaining the critical physical ingredients for droplet propulsion while remaining minimal and conceptually simple. But its underlying mathematical characteristics should not be overlooked. In fact, understanding whether potential peculiar behaviors result from modeling shortcomings or are an intrinsic feature of the physico-chemical problem is a fundamental challenge, and the well-posedness of the chemical transport problem provides an enlightening illustration.

Absent any bulk chemical relaxation, the existence of a steady state solution (propelling or not) requires transporting the released solute away from the droplet's surface. As for the classical problem of a sedimenting heat-/mass-releasing sphere (Acrivos & Taylor 1962), a fundamental dichotomy arises between diffusion-dominated transport at $\mathcal{O}(R)$ -distances and a convection-driven

Topological defect:
a point or line
singularity in the local
directional ordering of
a liquid crystal

region at $r = \mathcal{O}(D/V)$. For $VR/D \ll 1$, these two scales are clearly separated, introducing a far-field boundary layer whose existence in fact conditions the bifurcation and onset of self-propulsion (Vélarde et al. 1996, Farutin & Misbah 2021).

Finite-Pe self-propulsion of homogeneous active droplets (or phoretic particles) develops from an isotropic state with no fluid or droplet motion and where the solute can only be transported away by diffusion. Such balance is possible in 3D, albeit precariously, but breaks down as soon as chemical transport is geometrically restricted (e.g., in 2D or in a channel), and a regularizing mechanism is required, such as time dependence (Sondak et al. 2016) or convection (Yariv 2017). Such technical yet fundamental difficulties are not present when the solute concentration spontaneously relaxes to equilibrium in the bulk fluid (e.g., Yoshinaga et al. 2012), which introduces an exponential chemical screening.

6.3. Coupling with the Droplet Internal Dynamics and Control Opportunities

The fluid nature of the droplet is enough to understand the spontaneous onset of its motion or some of its complex dynamics, but its internal structure may introduce critical changes and controls that represent important challenges and opportunities for the field. The presence of a topological defect (Krüger et al. 2016b) or an internal core (Hokmabad et al. 2019) in LC droplets or shells can promote curly, helicoidal, or meandering trajectories as a result of the coupling of the droplet motion with an internal polarity (Morozov & Michelin 2019b). Helical propulsion can also be directly achieved with nonnematic droplets (Hokmabad et al. 2022a) or by using the internal chirality of cholesteric LC droplets (Yamamoto & Sano 2017). Encapsulating solid particles in the droplet enhances the self-propulsion velocity by providing yet another internal polarization of the droplet structure (Cheon et al. 2021). Multicomponent droplets also gain, at least transiently, an internal polarity due to the differential dissolution and phase separation of their individual components (Li et al. 2020, Wang et al. 2021).

Beyond the need for and interest in a fundamental understanding, research into the influence of the droplet's internal properties on its motion is motivated by its control opportunities. By incorporating chiral molecular motors into a nematic LC, Lancia et al. (2019) prepared cholesteric droplets whose helical trajectories and handedness could be controlled by an external light. In a similar spirit, light-controlled switches of the conformation of the surfactant covering the droplet surface can be used to change the droplet solubilization rate and produce run-and-halt motions (Ryabchun et al. 2021). The sensitive conditions for the internal kinetics of chemically reacting droplets can also be used to control the propulsion mode, such as the pH of the outer fluid (Ban et al. 2013) or the internal state of the oscillatory BZ reaction (Kitahata et al. 2011, Thutupalli & Herminghaus 2013, Suematsu et al. 2021).

SUMMARY POINTS

1. Chemically active droplets emit, consume, or alter surfactant monomers or micelles; they exploit the nonlinear convective transport by the surface-driven flows resulting from these solutes' gradients in order to self-propel.
2. Due to this nonlinear coupling and their isotropy, their individual motions are fundamentally different from other (asymmetric) chemically active colloids.
3. Their dual hydrochemical footprint leads to complex interactions with other droplets or confining boundaries.

FUTURE ISSUES

1. What are the origins and characteristics of the individual complex trajectories and chaotic-like dynamics of isolated droplets observed in experiments?
2. How can we model the dynamics of many active droplets or within complex geometries, while retaining the intrinsic nonlinearity of the hydrochemical coupling? Are direct numerical simulations the only resort? If so, what are the most adapted methods to accurately treat the nonlinear coupling and moving droplet boundaries?
3. What is the influence of active droplets' geometric environment on their motion? How relevant are bulk models for understanding observations?
4. Existing models place much focus on hydrodynamic and transport modeling. Are the details of the physical chemistry involved important? What are the role and features of the surfactant dynamics at the densely covered interface?
5. Can the motion of active droplets be controlled? If so, how and for which purposes can they realistically be used for engineering applications?

DISCLOSURE STATEMENT

The author is not aware of any biases that might be perceived as affecting the objectivity of this review.

ACKNOWLEDGMENTS

I am grateful to Eric Lauga and Cecile Cottin Bizonne for their careful feedback on the manuscript, to Olivier Dauchot for providing some of the experimental photos included here, and to Denis Bartolo, Matvey Morozov, Ory Schnitzer, Udi Yariv and Jasna Brujic, along with the aforementioned individuals, for many insightful discussions on the dynamics of active droplets. This work has received funding from the European Research Council under the European Union's Horizon 2020 research and innovation program (grant agreement 714027).

LITERATURE CITED

- Acrivos A, Taylor TD. 1962. Heat and mass transfer from single spheres in Stokes flow. *Phys. Fluids* 5(4):387
- Anderson JL. 1989. Colloid transport by interfacial forces. *Annu. Rev. Fluid Mech.* 21:61–99
- Ban T, Tani K, Nakata H, Okano Y. 2014. Self-propelled droplets for extracting rare-earth metal ions. *Soft Matter* 10(33):6316–20
- Ban T, Yamada T, Aoyama A, Takagi Y, Okano Y. 2012. Composition-dependent shape changes of self-propelled droplets in a phase-separating system. *Soft Matter* 8(14):3908–16
- Ban T, Yamagami T, Nakata H, Okano Y. 2013. pH-dependent motion of self-propelled droplets due to Marangoni effect at neutral pH. *Langmuir* 29(8):2554–61
- Banno T, Kuroha R, Toyota T. 2011. pH-sensitive self-propelled motion of oil droplets in the presence of cationic surfactants containing hydrolyzable ester linkages. *Langmuir* 28(2):1190–95
- Banno T, Miura S, Kuroha R, Toyota T. 2013. Mode changes associated with oil droplet movement in solutions of gemini cationic surfactants. *Langmuir* 29(25):7689–96
- Berg HC. 1975. Chemotaxis in bacteria. *Annu. Rev. Biophys. Bioeng.* 4:119–36
- Berg HC, Anderson RA. 1973. Bacteria swim by rotating their flagellar filaments. *Nature* 245(5425):380–82
- Boniface D, Cottin-Bizonne C, Detcheverry F, Ybert C. 2021. Role of Marangoni forces in the velocity of symmetric interfacial swimmers. *Phys. Rev. Fluids* 6:104006

- Boniface D, Cottin-Bizonne C, Kervil R, Ybert C, Detcheverry F. 2019. Self-propulsion of symmetric chemically active particles: point-source model and experiments on camphor disks. *Phys. Rev. E* 99:062605
- Brennen C, Winet H. 1977. Fluid mechanics of propulsion by cilia and flagella. *Annu. Rev. Fluid Mech.* 9:339-98
- Browne K, Walker D, Bishop K, Grzybowski B. 2010. Self-division of macroscopic droplets: partitioning of nanosized cargo into nanoscale micelles. *Angew. Chem. Int. Ed.* 49(38):6756-59
- Chen Y, Chong KL, Liu L, Verzicco R, Lohse D. 2021. Instabilities driven by diffusiophoretic flow on catalytic surfaces. *J. Fluid Mech.* 919:A10
- Cheon SI, Silva LBC, Khair AS, Zarzar LD. 2021. Interfacially-adsorbed particles enhance the self-propulsion of oil droplets in aqueous surfactant. *Soft Matter* 17(28):6742-50
- Childress S. 1981. *Mechanics of Swimming and Flying*. Cambridge, UK: Cambridge Univ. Press
- de Blois C, Bertin V, Suda S, Ichikawa M, Reyssat M, Dauchot O. 2021. Swimming droplets in 1D geometries: an active Bretherton problem. *Soft Matter* 17(27):6646-60
- de Blois C, Reyssat M, Michelin S, Dauchot O. 2019. Flow field around a confined active droplet. *Phys. Rev. Fluids* 4:054001
- de Corato M, Pagonabarraga I, Abdelmohsen LKEA, Sánchez S, Arroyo M. 2020. Spontaneous polarization and locomotion of an active particle with surface-mobile enzymes. *Phys. Rev. Fluids* 5:122001
- Desai N, Michelin S. 2021. Instabilities and self-propulsion of active droplets along a wall. *Phys. Rev. Fluids* 6:114103
- Dey R, Bunes CM, Hokmabad BV, Jin C, Maass CC. 2022. Oscillatory rheotaxis of artificial swimmers in microchannels. *Nat. Commun.* 13:2952
- Dreyfus R, Baudry J, Roper ML, Fermigier M, Stone HA, Bibette J. 2005. Microscopic artificial swimmers. *Nature* 437(7060):862-65
- Duan W, Wang W, Das S, Yadav V, Mallouk TE, Sen A. 2015. Synthetic nano- and micromachines in analytical chemistry: sensing, migration, capture, delivery, and separation. *Annu. Rev. Anal. Chem.* 8:311-33
- Dwivedi P, Shrivastava A, Pillai D, Mangal R. 2021a. Rheotaxis of active droplets. *Phys. Fluids* 33(8):082108
- Dwivedi P, Si BR, Pillai D, Mangal R. 2021b. Solute induced jittery motion of self-propelled droplets. *Phys. Fluids* 33(2):022103
- Ender H, Froin AK, Rehage H, Kierfeld J. 2021. Surfactant-loaded capsules as Marangoni microswimmers at the air-water interface: symmetry breaking and spontaneous propulsion by surfactant diffusion and advection. *Eur. Phys. J. E* 44:21
- Farutin A, Misbah C. 2021. Singular bifurcations: a regularization theory. arXiv:2112.12094 [cond-mat.soft]
- Herminghaus S, Maass CC, Krüger C, Thutupalli S, Goehring L, Bahr C. 2014. Interfacial mechanisms in active emulsions. *Soft Matter* 10(36):7008-22
- Hirono A, Toyota T, Asakura K, Banno T. 2018. Locomotion mode of micrometer-sized oil droplets in solutions of cationic surfactants having ester or ether linkages. *Langmuir* 34(26):7821-26
- Hokmabad BV, Baldwin KA, Krüger C, Bahr C, Maass CC. 2019. Topological stabilization and dynamics of self-propelling nematic shells. *Phys. Rev. Lett.* 123:178003
- Hokmabad BV, Dey R, Jalaal M, Mohanty D, Almukambetova M, et al. 2021. Emergence of bimodal motility in active droplets. *Phys. Rev. X* 11:011043
- Hokmabad BV, Nishide A, Ramesh P, Maass CC. 2022a. Spontaneously rotating clusters of active droplets. *Soft Matter* 18:2731-41
- Hokmabad BV, Agudo-Canalejo J, Saha S, Golestanian R, Maass CC. 2022b. Chemotactic self-caging in active emulsions. *PNAS* 119(24):e2122269119
- Hu WF, Lin TS, Rafai S, Misbah C. 2019. Chaotic swimming of phoretic particles. *Phys. Rev. Lett.* 123:238004
- Izri Z, van der Linden MN, Michelin S, Dauchot O. 2014. Self-propulsion of pure water droplets by spontaneous Marangoni-stress-driven motion. *Phys. Rev. Lett.* 113:248302
- Izzet A, Moerman PG, Gross P, Groenewold J, Hollingsworth AD, et al. 2020. Tunable persistent random walk in swimming droplets. *Phys. Rev. X* 10:021035
- Jin C, Chen Y, Maass CC, Majthijssen AJTM. 2021. Collective entrainment and confinement amplify transport by schooling microswimmers. *Phys. Rev. Lett.* 127:088006
- Jin C, Hokmabad BV, Baldwin KA, Maass CC. 2018. Chemotactic droplet swimmers in complex geometries. *J. Phys. Condens. Matter* 30(5):054003

- Jin C, Krüger C, Maass CC. 2017. Chemotaxis and autochemotaxis of self-propelling droplet swimmers. *PNAS* 114(20):5089–94
- Jin C, Vachier J, Bandyopadhyay S, Macharashvili T, Maass CC. 2019. Fine balance of chemotactic and hydrodynamic torques: when microswimmers orbit a pillar just once. *Phys. Rev. E* 100:040601
- Jurado-Sánchez B, Sattayasamitsathit S, Gao W, Santos L, Fedorak Y, et al. 2014. Self-propelled activated carbon janus micromotors for efficient water purification. *Small* 11(4):499–506
- Jurado-Sánchez B, Wang J. 2018. Micromotors for environmental applications: a review. *Environ. Sci. Nano* 5(7):1530–44
- Kagan D, Laocharoensuk R, Zimmerman M, Clawson C, Balasubramanian S, et al. 2010. Rapid delivery of drug carriers propelled and navigated by catalytic nanoshuttles. *Small* 6(23):2741–47
- Kasuo Y, Kitahata H, Koyano Y, Takinoue M, Asakura K, Banno T. 2019. Start of micrometer-sized oil droplet motion through generation of surfactants. *Langmuir* 35(41):13351–55
- Katuri J, Uspal WE, Simmchen J, Miguel-López A, Sánchez S. 2018. Cross-stream migration of active particles. *Sci. Adv.* 4(1):eaao1755
- Kim S, Karrila SJ. 1991. *Microhydrodynamics*. Stoneham, MA: Butterworth-Heinemann
- Kitahata H, Yoshinaga N, Nagai KH, Sumino Y. 2011. Spontaneous motion of a droplet coupled with a chemical wave. *Phys. Rev. E* 84:015101
- Krüger C, Bahr C, Herminghaus S, Maass CC. 2016a. Dimensionality matters in the collective behaviour of active emulsions. *Eur. Phys. J. E* 39:64
- Krüger C, Klös G, Bahr C, Maass CC. 2016b. Curling liquid crystal microswimmers: a cascade of spontaneous symmetry breaking. *Phys. Rev. Lett.* 117:048003
- Lancia F, Yamamoto T, Ryabchun A, Yamaguchi T, Sano M, Katsonis N. 2019. Reorientation behavior in the helical motility of light-responsive spiral droplets. *Nat. Commun.* 10:5238
- Lauga E. 2016. Bacterial hydrodynamics. *Annu. Rev. Fluid Mech.* 48:105–30
- Lauga E. 2020. *The Fluid Dynamics of Cell Motility*. Cambridge, UK: Cambridge Univ. Press
- Lauga E, Powers TR. 2009. The hydrodynamics of swimming microorganisms. *Rep. Prog. Phys.* 72(9):096601
- Li M, Brinkmann M, Pagonabarraga I, Seemann R, Fleury JB. 2018. Spatiotemporal control of cargo delivery performed by programmable self-propelled janus droplets. *Commun. Phys.* 1:23
- Li M, Hosseinzadeh M, Pagonabarraga I, Seemann R, Brinkmann M, Fleury JB. 2020. Kinetics of active water/ethanol janus droplets. *Soft Matter* 16(29):6803–11
- Lighthill J. 1976. Flagellar hydrodynamics. *SLAM Rev.* 18(2):161–230
- Lin TS, Hu WF, Misbah C. 2020. A direct Poisson solver in spherical geometry with an application to diffusiophoretic problems. *J. Comp. Phys.* 409:109362
- Lippner K, Benzaquen M, Michelin S. 2020a. Bouncing, chasing, or pausing: asymmetric collisions of active droplets. *Phys. Rev. Fluids* 5:032201
- Lippner K, Benzaquen M, Michelin S. 2021. Alignment and scattering of colliding active droplets. *Soft Matter* 17(2):365–75
- Lippner K, Morozov M, Benzaquen M, Michelin S. 2020b. Collisions and rebounds of chemically active droplets. *J. Fluid Mech.* 886:A17
- Maass CC, Krüger C, Herminghaus S, Bahr C. 2016. Swimming droplets. *Annu. Rev. Condens. Matter Phys.* 7:171–93
- Marchetti MC, Joanny JF, Ramaswamy S, Liverpool TB, Prost J, et al. 2013. Hydrodynamics of soft active matter. *Rev. Mod. Phys.* 85(3):1143–89
- Marcos, Fu HC, Powers TR, Stocker R. 2012. Bacterial rheotaxis. *PNAS* 109(13):4780–85
- Meredith CH, Moerman PG, Groenewold J, Chiu YJ, Kegel WK, et al. 2020. Predator–prey interactions between droplets driven by non-reciprocal oil exchange. *Nat. Chem.* 12(12):1136–42
- Michelin S, Lauga E, Bartolo D. 2013. Spontaneous autophoretic motion of isotropic particles. *Phys. Fluids* 25(6):061701
- Misbah C, Rizvi MS, Hu WF, Lin TS, Rafai S, Farutin A. 2021. Universal trajectories of motile particles driven by chemical activity. arXiv:2112.13801 [cond-mat.soft]
- Moerman PG. 2019. *Dynamics of active droplets and free jointed colloidal trimers*. PhD Thesis, Utrecht Univ., Utrecht, Neth.

- Moerman PG, Moyses HW, van der Wee EB, Grier DG, van Blaaderen A, et al. 2017. Solute-mediated interactions between active droplets. *Phys. Rev. E* 96:032607
- Moran JL, Posner JD. 2017. Phoretic self-propulsion. *Annu. Rev. Fluid Mech.* 49:511–40
- Morozov M. 2020. Adsorption inhibition by swollen micelles may cause multistability in active droplets. *Soft Matter* 16(24):5624–32
- Morozov M, Michelin S. 2018. Self-propulsion near the onset of Marangoni instability of deformable active droplets. *J. Fluid Mech.* 860:711–38
- Morozov M, Michelin S. 2019a. Nonlinear dynamics of a chemically-active drop: from steady to chaotic self-propulsion. *J. Chem. Phys.* 150(4):044110
- Morozov M, Michelin S. 2019b. Orientational instability and spontaneous rotation of active nematic droplets. *Soft Matter* 15(39):7814–22
- Nelson BJ, Kaliakatsos IK, Abbott JJ. 2010. Microrobots for minimally invasive medicine. *Annu. Rev. Biomed. Eng.* 12:55–85
- Pak OS, Lauga E. 2015. Theoretical models of low-Reynolds-number locomotion. In *Fluid–Structure Interactions in Low-Reynolds-Number Flows*, ed. C Duprat, HA Stone, pp. 100–67. London: R. Soc. Chem.
- Palacci J, Sacanna S, Abramian A, Barral J, Hanson K, et al. 2015. Artificial rheotaxis. *Sci. Adv.* 1(4):e140021
- Palagi S, Fischer P. 2018. Bioinspired microrobots. *Nat. Rev. Mater.* 3(6):113–24
- Paxton WF, Kistler KC, Olmeda CC, Sen A, Angelo SKS, et al. 2004. Catalytic nanomotors: autonomous movement of striped nanorods. *J. Am. Chem. Soc.* 126(41):13424–31
- Peddireddy K, Kumar P, Thutupalli S, Herminghaus S, Bahr C. 2012. Solubilization of thermotropic liquid crystal compounds in aqueous surfactant solutions. *Langmuir* 28(34):12426–31
- Picella F, Michelin S. 2022. Confined self-propulsion of isotropic active colloids. *J. Fluid Mech.* 933:A27
- Rednikov AY, Ryazantsev YS, Vélarde MG. 1994a. Drop motion with surfactant transfer in a homogeneous surrounding. *Phys. Fluids* 6(2):451–68
- Rednikov AY, Ryazantsev YS, Vélarde MG. 1994b. Drop motion with surfactant transfer in an inhomogeneous medium. *Int. J. Heat Mass Transf.* 37:361–74
- Rednikov AY, Ryazantsev YS, Vélarde MG. 1994c. On the development of translational subcritical Marangoni instability for a drop with uniform internal heat generation. *J. Colloid Interface Sci.* 164(1):168–80
- Ryabchun A, Babu D, Movilli J, Plamont R, Katsonis N. 2021. Run-and-halt behavior of motile droplets in response to light. ChemRxiv 14417552. <https://doi.org/10.26434/chemrxiv.14417552.v1>
- Saha S, Yariv E, Schnitzer O. 2021. Isotropically active colloids under uniform force fields: from forced to spontaneous motion. *J. Fluid Mech.* 916:A47
- Schmitt M, Stark H. 2013. Swimming active droplet: a theoretical analysis. *EPL* 101(4):44008
- Schmitt M, Stark H. 2016. Marangoni flow at droplet interfaces: three-dimensional solution and applications. *Phys. Fluids* 28(1):012106
- Seemann R, Fleury JB, Maass CC. 2016. Self-propelled droplets. *Eur. Phys. J. Spec. Top.* 225(11–12):2227–40
- Sondak D, Hawley C, Heng S, Vinsonhaler R, Lauga E, Thiffeault JL. 2016. Can phoretic particles swim in two dimensions? *Phys. Rev. E* 94:062606
- Suda S, Suda T, Ohmura T, Ichikawa M. 2021. Straight-to-curvilinear motion transition of a swimming droplet caused by the susceptibility to fluctuations. *Phys. Rev. Lett.* 127:088005
- Suematsu NJ, Mori Y, Amemiya T, Nakata S. 2016. Oscillation of speed of a self-propelled Belousov–Zhabotinsky droplet. *J. Phys. Chem. Lett.* 7(17):3424–28
- Suematsu NJ, Mori Y, Amemiya T, Nakata S. 2021. Spontaneous mode switching of self-propelled droplet motion induced by a clock reaction in the Belousov–Zhabotinsky medium. *J. Phys. Chem. Lett.* 12(31):7526–30
- Suematsu NJ, Saikusa K, Nagata T, Izumi S. 2019. Interfacial dynamics in the spontaneous motion of an aqueous droplet. *Langmuir* 35(35):11601–7
- Suga M, Suda S, Ichikawa M, Kimura Y. 2018. Self-propelled motion switching in nematic liquid crystal droplets in aqueous surfactant solutions. *Phys. Rev. E* 97:062703
- Thutupalli S, Geyer D, Singh R, Adhikari R, Stone HA. 2018. Flow-induced phase separation of active particles is controlled by boundary conditions. *PNAS* 115(21):5403–8
- Thutupalli S, Herminghaus S. 2013. Tuning active emulsion dynamics via surfactants and topology. *Eur. Phys. J. E* 36:91

- Thutupalli S, Seemann R, Herminghaus S. 2011. Swarming behavior of simple model squirmers. *New J. Phys.* 13(7):073021
- Tomlinson C. 1862. II. On the motions of camphor on the surface of water. *Proc. R. Soc. Lond.* 11:575–77
- Toyota T, Maru N, Hanczyc MM, Ikegami T, Sugawara T. 2009. Self-propelled oil droplets consuming “fuel” surfactant. *J. Am. Chem. Soc.* 131(14):5012–13
- Toyota T, Tsuba H, Yamada K, Takakura K, Ikegami T, Sugawara T. 2006. Listeria-like motion of oil droplets. *Chem. Lett.* 35(7):708–9
- Velarde MG, Rednikov AY, Ryazantsev YS. 1996. Drop motions and interfacial instability. *J. Phys. Condens. Matter* 8(47):9233–47
- Vilfan M, Potočnik A, Kavčič B, Osterman N, Poberaj I, et al. 2009. Self-assembled artificial cilia. *PNAS* 107(5):1844–47
- Wang X, Zhang R, Mozaffari A, de Pablo JJ, Abbott NL. 2021. Active motion of multiphase oil droplets: emergent dynamics of squirmers with evolving internal structure. *Soft Matter* 17(10):2985–93
- Yabunaka S, Yoshinaga N. 2016. Collision between chemically driven self-propelled drops. *J. Fluid Mech.* 806:205–33
- Yamamoto T, Sano M. 2017. Chirality-induced helical self-propulsion of cholesteric liquid crystal droplets. *Soft Matter* 13(18):3328–33
- Yariv E. 2016. Wall-induced self-diffusiophoresis of active isotropic colloids. *Phys. Rev. Fluids* 1:032101
- Yariv E. 2017. Two-dimensional phoretic swimmers: the singular weak-advection limits. *J. Fluid Mech.* 816:R3
- Yariv E, Kaynan U. 2017. Phoretic drag reduction of chemically active homogeneous spheres under force fields and shear flows. *Phys. Rev. Fluids* 2:012201
- Yi Y, Sanchez L, Gao Y, Yu Y. 2016. Janus particles for biological imaging and sensing. *Analyst* 141(12):3526–39
- Yoshinaga N. 2014. Spontaneous motion and deformation of a self-propelled droplet. *Phys. Rev. E* 89:012913
- Yoshinaga N, Nagai KH, Sumino Y, Kitahata H. 2012. Drift instability in the motion of a fluid droplet with a chemically reactive surface driven by Marangoni flow. *Phys. Rev. E* 86:016108
- Zhang L, Abbott JJ, Dong L, Peyer KE, Kratochvil BE, et al. 2009. Characterizing the swimming properties of artificial bacterial flagella. *Nano Lett.* 9(10):3663–67



Contents

Flow Computation Pioneer Irmgard Flügge-Lotz (1903–1974) <i>Jonathan B. Freund</i>	1
Fluid Mechanics in France in the First Half of the Twentieth Century <i>François Charru</i>	11
New Insights into Turbulent Spots <i>Xiaobua Wu</i>	45
Self-Propulsion of Chemically Active Droplets <i>Sébastien Michelin</i>	77
Submesoscale Dynamics in the Upper Ocean <i>John R. Taylor and Andrew F. Thompson</i>	103
Immersed Boundary Methods: Historical Perspective and Future Outlook <i>Roberto Verzicco</i>	129
Motion in Stratified Fluids <i>Rishabh V. More and Arezoo M. Ardekani</i>	157
The Flow Physics of Face Masks <i>Rajat Mittal, Kenneth Breuer, and Jung Hee Seo</i>	193
Advancing Access to Cutting-Edge Tabletop Science <i>Michael F. Schatz, Pietro Cicuta, Vernita D. Gordon, Teuta Pilizota, Bruce Rodenborn, Mark D. Shattuck, and Harry L. Swinney</i>	213
Cerebrospinal Fluid Flow <i>Douglas H. Kelley and John H. Thomas</i>	237
Fluid Dynamics of Polar Vortices on Earth, Mars, and Titan <i>Darryn W. Waugh</i>	265
Dynamics of Three-Dimensional Shock-Wave/Boundary-Layer Interactions <i>Datta V. Gaitonde and Michael C. Adler</i>	291

Gas-Liquid Foam Dynamics: From Structural Elements to Continuum Descriptions <i>Peter S. Stewart and Sascha Hilgenfeldt</i>	323
Recent Developments in Theories of Inhomogeneous and Anisotropic Turbulence <i>J.B. Marston and S.M. Tobias</i>	351
Icebergs Melting <i>Claudia Cenedese and Fiamma Straneo</i>	377
The Fluid Mechanics of Deep-Sea Mining <i>Thomas Peacock and Raphael Ouillon</i>	403
A Perspective on the State of Aerospace Computational Fluid Dynamics Technology <i>Mori Mani and Andrew J. Dorgan</i>	431
Particle Rafts and Armored Droplets <i>Suzie Protière</i>	459
Evaporation of Sessile Droplets <i>Stephen K. Wilson and Hannab-May D'Ambrosio</i>	481
3D Lagrangian Particle Tracking in Fluid Mechanics <i>Andreas Schröder and Daniel Schanz</i>	511
Linear Flow Analysis Inspired by Mathematical Methods from Quantum Mechanics <i>Luca Magri, Peter J. Schmid, and Jonas P. Moeck</i>	541
Transition to Turbulence in Pipe Flow <i>Marc Avila, Dwight Barkley, and Björn Hof</i>	575
Turbulent Rotating Rayleigh–Bénard Convection <i>Robert E. Ecke and Olga Shishkina</i>	603
Nonidealities in Rotating Detonation Engines <i>Venkat Raman, Supraj Prakash, and Mirko Gamba</i>	639
Elasto-Inertial Turbulence <i>Yves Dubief, Vincent E. Terrapon, and Björn Hof</i>	675
Sharp Interface Methods for Simulation and Analysis of Free Surface Flows with Singularities: Breakup and Coalescence <i>Christopher R. Anthony, Hansol Wee, Visbrut Garg, Sumeet S. Thete, Pritish M. Kamat, Brayden W. Wagoner, Edward D. Wilkes, Patrick K. Notz, Alvin U. Chen, Ronald Suryo, Krisbharaj Sambath, Jayanta C. Panditaratne, Ying-Chih Liao, and Osman A. Basaran</i>	707

Indexes

Cumulative Index of Contributing Authors, Volumes 1–55	749
Cumulative Index of Article Titles, Volumes 1–55	760

Errata

An online log of corrections to *Annual Review of Fluid Mechanics* articles may be found at <http://www.annualreviews.org/errata/fluid>